Preprint PFC/JA-83-16

DISPERSION CHARACTERISTICS OF A FREE ELECTRON LASER WITH A LINEARLY POLARIZED WIGGLER AND AXIAL GUIDE FIELD

Y.Z. Yin and G. Bekefi

Plasma Fusion Center and
Research Laboratory of Electronics
Massachusetts Institute of Technology
Cambridge, MA. 02139

May 1983

DISPERSION CHARACTERISTICS OF A FREE ELECTRON LASER WITH A LINEARLY POLARIZED WIGGLER AND AXIAL GUIDE FIELD

Y.Z. Yin† and G. Bekefi

Department of Physics and Research Laboratory of Electronics

Massachusetts Institute of Technology

Cambridge, Massachusetts 02139

ABSTRACT

Calculations of the dispersion characteristics of a free electron laser with a linearly polarized wiggler magnetic field and an axial guide magnetic field have been carried out in the collective (Raman) regime for a cold, relativistic electron beam passing through a parallel-plate waveguide. The linear growth rate and efficiency of the TE and TEM waveguide modes have been computed for radiation in the centimeter and millimeter wavelength ranges.

†Permanent address: Institute of Electronics, Academia Sinica, Beijing, People's Republic of China

I. INTRODUCTION

Many theoretical studies[1-5] have been devoted to free electron lasers (FEL) comprised of an electron stream traversing a periodic, circularly polarized magnetic (wiggler) field, as can be generated[6-7] with bifilar, helical, current-carrying wires. The electron dynamics in these systems exhibit simple properties that have considerable theoretical appeal. However, from the experimental point of view large amplitude, circularly polarized wiggler fields are difficult to attain because of the large currents that are required in their windings; and for long pulse or steady-state operation, bifilar conductors may be entirely out of the question. In view of the above, studies of free electron lasers have begun[8-11] in which the electron beam is subjected to a periodic, linearly polarized transverse magnetic field such as can be produced, for example, by an assembly of permanent magnets illustrated in Fig. 1a. Indeed, the use of samarium-cobalt as the magnet material has lead to a new generation of magnetic wiggler systems.[12,13]

In this paper we calculate from appropriate fluid equations dispersion characteristics of the FEL instability in the collective (Raman) regime for the case of a cold monoenergetic electron beam. The geometry is illustrated in Fig. 1a. An electron beam of velocity v_o traverses a parallel-plate waveguide immersed in a static magnetic field which in our one dimensional model (applicable to sufficiently small transverse quiver motions of the electrons) can be approximated by

$$\vec{B} = \hat{z}B_{\parallel} + \hat{x}B_w\cos(k_w z) \tag{1}$$

Here $B_{\parallel}$ is the amplitude of the guide field; and B_w and $k_w=2\pi/\ell$ are the amplitude and wavenumber of the wiggler field, respectively (ℓ is the spatial periodicity). The axial guide field $B_{\parallel}$ has a two-fold purpose. First, it confines[14] the electrons against the radial space-charge forces and thereby permits the propagation of high current-density beams. And secondly, it can enhance[15,16,17]

the growth rate of the FEL instability by exploiting the resonance between the electron cyclotron frequency $eB_{\parallel}/m_o c\gamma_o$ in guide field $B_{\parallel}$, and the frequency $k_w v_o$ associated with the wiggler field B_w ($\gamma_o=(1-\beta_0^2)^{-\frac{1}{2}}$, $\beta_o=v_o/c$).

In our model the electron beam is allowed to fill uniformly the parallel plate waveguide shown in Fig. 1a. The electromagnetic perturbations, taken to vary in the propagation direction z as $\exp(ikz-i\omega t)$, are assumed to be short wavelength such that spatial variations transverse to z can be neglected; that is, $\partial/\partial x$, $\partial/\partial y << \partial/\partial z$. Subject to these conditions we shall derive dispersion equations for two modes of polarizations. (i) A transverse electric (TE) mode with $\vec{E}=\hat{y}E_y$, $\vec{B}=\hat{x}B_x+\hat{z}B_z$ and (ii) a transverse electromagnetic (TEM) mode with $\vec{E}=\hat{x}E_x$, $\vec{B}=\hat{y}B_y$. We will show that the two modes have different growth rates. Indeed the FEL instability associated with the TEM mode exists only by virtue of the presence of the axial guide field $B_{\parallel}$ which couples the cyclotron motion of the electrons to their quiver motion in the wiggler field B_w.

In section II we discuss the steady state beam dynamics in the wiggler and guide fields. In section III we derive the dispersion equations for the FEL instability for the two modes of polarization stated above. Finally, section IV will be devoted to giving numerical examples of the radiation frequency, phase velocity and the instability growth rate. Estimates of the free electron laser efficiency will also be given. The FEL parameters have been chosen to yield radiation in the centimeter and millimeter wavelength regions using both low and high velocity electron beams. Table 1 gives a summary of the FEL parameters. At low, essentially nonrelativistic velocities ($\gamma_o \simeq 1$), the radiation wavelength is roughly equal to the wiggler period ℓ, as is typical of UBITRONS.[18] Here the efficiency is large and operation is possible with low current density beams that can be obtained from electron guns using thermionic cathodes. At high velocities, the radiation wavelength is approximately equal to $\ell/2\gamma_0^2$; now the efficiency is small and the system must be operated

using high current density beams (see Table 1) like those generated by field emission cathodes.[19,20]

II. ELECTRON MOTION IN THE WIGGLER AND GUIDE FIELDS

Because of the discreteness of the magnets shown in Fig 1a, the wiggler magnetic field exhibits harmonics of the fundamental period ℓ having considerable amplitude. In practice,[4] the magnet arrangement illustrated in Fig. 1b removes the third harmonic and all even harmonics, with the result that the field approaches closely the periodic vacuum field

$$\begin{aligned} B_x^0 &= B_w \cosh(k_w x)\cos(k_w z) \\ B_y^0 &= 0 \\ B_z^0 &= - B_w \sinh(k_w x)\sin(k_w z) \end{aligned} \tag{2}$$

which satisfies $\nabla\times\vec{B} = \nabla\cdot\vec{B} = 0$. As a result the equations of motion of an electron of charge -e and rest mass m_o are,

$$\begin{aligned} \frac{dv_x^0}{dt} &= - \Omega_{\shortparallel} v_y^0 + \Omega_w v_y^0 \sinh(k_w x)\sin(k_w z) \\ \frac{dv_y^0}{dt} &= \Omega_{\shortparallel} v_x^0 - \Omega_w v_x^0 \sinh(k_w x)\sin(k_w z) - \Omega_w v_z^0 \cosh(k_w x)\cos(k_w z) \\ \frac{dv_z^0}{dt} &= \Omega_w v_y^0 \cosh(k_w x)\cos(k_w z), \end{aligned} \tag{3}$$

Here $\Omega_{\shortparallel} = eB_{\shortparallel}/\gamma_0 m_0 c$ and $\Omega_w = eB_w/\gamma_0 m_0 c$ are the cyclotron frequencies in the guide magnetic field $B_{\shortparallel}$ and wiggler magnetic field B_w, respectively ($\gamma_0 = (1-\beta_0^2)^{-\frac{1}{2}}$; $\beta_0 = v_0/c$).

Equations (3) has been solved numerically by the variable-step method of Adam[21] using the facilities of the MIT Computer Information Processing Center. Figure 2a shows the projection onto the x-y plane of an electron trajectory for the case of an electron starting on axis $x_0=y_0=z_0=0$ with velocity $\vec{v}=\hat{z}v_0$ equal to 2.33×10^{10}cm/s (beam voltage V=300kV). It is guided by an axial magnetic field $B_{\shortparallel}$ equal to 5kG and perturbed by a wiggler field having a periodic-

ity ℓ=1.0cm and amplitude of 0.5kG. Figure 2b shows a plot of electron displacement $r=(x^2+y^2)^{\frac{1}{2}}$ as a function of axial position. The motion is quasi-periodic. When the initial electron position is displaced from the center, the quasi-periodic oscillations are accompanied by a drift. This $\vec{B}\times\nabla\vec{B}/|B^2|$ drift results from the combined presence of the uniform axial magnetic field $\vec{B}_{\parallel}$ and the nonuniform wiggler field $\vec{B}_w$. Figure 3 illustrates the situation for the case when the initial electron position is given by x_0=0.1cm, $y_0=z_0=0$; the drift along the negative y direction is now clearly discernible. We note that the drift represents a major drawback when a linearly polarized wiggler and a guide field act simultaneously on a beam electron.[22] Moreover, the drift exhibits a resonance similar to that which occurs in the quiver motion[15,16,17] of the electrons. This problem is not encountered with helical wigglers. However, when the inequality

$$q \equiv |\Omega_w/(\Omega_{\parallel} - k_w v_0)| << 1 \qquad (4)$$

is satisfied, the drift and the oscillatory amplitudes are reasonably small. Figure 4 shows plots as a function of B_w and $B_{\parallel}$ of the combined drift plus quiver motion after an electron traverses a one meter long section of wiggler field and guide field. At a distance z≈100cm the maximum excursion for the cases shown in Fig. 4 is y_{max}≈1cm. The corresponding value q of Eq. (4) equals 0.3. Thus, even though q is quite substantial, the electron excursion from the axis is not excessively large.

Subject to the above inequality, $\vec{B}_w$ of Eq. (2) becomes $\vec{B}_w=\hat{x}B_w\cos(k_w z) + \hat{z}B_{\parallel}$, and the equations of motion of an electron whose initial velocity at z=0 is $\vec{v}=\hat{x}(0) + \hat{y}(0) + \hat{z}v_0$ are then given by

$$v_x^0 = v_1\cos(k_w z) - v_1\cos\left(\frac{\Omega_{\parallel}}{v_0} z\right)$$

$$v_y^0 = v_2\sin(k_w z) - v_1\sin\left(\frac{\Omega_{\parallel}}{v_0} z\right) \qquad (5)$$

$$v_z^0 = v_0$$

$$x = \frac{v_1}{k_w v_0} \sin(k_w z) - \frac{v_1}{\Omega_{\parallel}} \sin\left(\frac{\Omega_{\parallel}}{v_0} z\right)$$

$$y = -\frac{v_2}{k_w v_0} \cos(k_w z) + \frac{v_1}{\Omega_{\parallel}} \cos\left(\frac{\Omega_{\parallel}}{v_0} z\right) \tag{6}$$

$$z = v_0 t$$

where

$$v_1 = \frac{\Omega_w \Omega_{\parallel} v_0}{\Omega_{\parallel}^2 - k_w^2 v_0^2} \quad , \quad v_2 = \frac{\Omega_w k_w v_0^2}{\Omega_{\parallel}^2 - k_w^2 v_0^2} \quad .$$

Henceforth, we shall assume that inequality (4) is applicable, and that the steady state motion of the electrons (in the absence of the RF fields) are given by Eqs. (5) and (6).

III. DISPERSION RELATIONS

The dispersion equations for a cold electron beam will be obtained by solving the relativistic equation of motion of the electrons

$$\frac{d\vec{v}}{dt} = -\frac{e}{m_o \gamma}\left[\vec{E} + \frac{\vec{v}}{c} \times (\vec{B} + \vec{B}^0) - \frac{\vec{v}}{c^2}(\vec{v}\cdot\vec{E})\right] \tag{7}$$

together with the equation of continuity

$$\nabla\cdot(N\vec{v}) + \frac{\partial N}{\partial t} = 0, \tag{8}$$

and the wave equation

$$\nabla\times(\nabla\times\vec{E}) + \frac{1}{c^2}\frac{\partial^2\vec{E}}{\partial t^2} + \frac{4\pi}{c^2}\frac{\partial\vec{J}}{\partial t} = 0. \tag{9}$$

Here $\vec{v}=\vec{v}^0+\vec{v}$ is the sum of the steady state and RF components of the particle velocity; $N=n_o+n$ is the sum of the steady state and RF components of the particle number density; $\vec{J}=-e(n_o+n)(\vec{v}_o+\vec{v})$ is the sum of the steady state and RF current density; $\gamma=(1-(|\vec{v}_o+\vec{v}|/c)^2)^{-\frac{1}{2}}$; and $\vec{E}$ and $\vec{B}$ are the RF electric and magnet-

ic fields respectively, associated with the radiation and space-charge fields. The sought-after dispersion equations are derived by linearizing the above equations and allowing all perturbed parameters to take the general form,

$$F = \sum_{n=-\infty}^{n=\infty} f_n \exp\left[i\left(k_n z - \omega t\right)\right] \tag{10}$$

with $k_n = k + nk_w$, $n = 0, \pm 1, \pm 2 + \ldots$. Here ω is the radiation frequency, k the radiation wavenumber, and $k_w = 2\pi/\ell$ the wave number of the wiggler with period ℓ.

1. TE Mode of Polarization

For the TE mode of polarization, the RF field components are $\vec{E} = \hat{y}E_y$ and $\vec{B} = \hat{x}B_x + \hat{z}B_z$. Linearizing Eq. (7) and assuming that all transverse oscillations are small such that $\partial/\partial x$, $\partial/\partial y << \partial/\partial z$, we obtain,

$$\left(\frac{\partial}{\partial t} + v_o \frac{\partial}{\partial z}\right) v_x = -\frac{e}{\gamma_o m_o}\left[\frac{1}{c} B_{\shortparallel} v_y + \frac{1}{c} v_y^0 B_z - \frac{1}{c^2} v_o v_x^0 E_\ell\right]$$

$$\left(\frac{\partial}{\partial t} + v_o \frac{\partial}{\partial z}\right) v_y = -\frac{e}{\gamma_o m_o}\left[E_y - \frac{1}{c} B_{\shortparallel} v_x + \frac{1}{c} v_o B_x - \frac{1}{c} v_x^0 B_z - \frac{1}{c^2} v_o v_y^0 E_\ell - \frac{\gamma_0^2}{c^3} v_o^2 B_x^0 v_z\right] \tag{11}$$

$$\left(\frac{\partial}{\partial t} + v_o \frac{\partial}{\partial z}\right) v_z = -\frac{e}{\gamma_o m_o}\left[-\frac{1}{c} B_x^0 v_y - \frac{1}{c} v_y^0 B_x - \frac{1}{c^2} v_o v_y^0 E_y + \frac{1}{\gamma_o^2} E_\ell\right]$$

where $\hat{z}E_\ell$ is the axial electric field associated with the RF space charge on the electron beam, and where γ of Eq. (7) has been approximated by

$$\gamma \simeq \gamma_o \left(1 + \gamma_o^2 \vec{v}^0 \cdot \vec{v}/c^2\right). \tag{12}$$

Substituting Eq. (10) in Eqs. (11) and using the orthogonality relation

$$\int_o^\ell \exp\left(ik_n z\right)\exp\left(-ik_m z\right)\, dz = \begin{cases} 0 & n \neq m \\ \ell & n = m \end{cases} \tag{13}$$

leads to the following expressions for the spatial harmonics of the perturbed velocities:

$$v_{xn} = - i \frac{e}{\gamma_o m_o \Omega_n} \left[\frac{B_{\parallel}}{c} v_{yn} - i \frac{v_2}{2c} \left(B_{zn-1} - B_{zn+1} \right) - \frac{v_o v_1}{2c^2} \left(E_{\ell n-1} + E_{\ell n+1} \right) \right]$$

$$v_{yn} = - i \frac{e}{\gamma_o m_o \Omega_n} \left[E_{yn} - \frac{B_{\parallel}}{c} v_{xn} + \frac{v_o}{c} B_{xn} - \frac{v_1}{2c} \left(B_{zn-1} + B_{zn+1} \right) + \right.$$

$$\left. i \frac{v_o v_2}{2c^2} \left(E_{\ell n-1} + E_{\ell n+1} \right) - \frac{\gamma_o^2 v_o^2 B_w}{2c^3} \left(v_{zn-1} + v_{zn+1} \right) \right] \qquad (14)$$

$$v_{zn} = - i \frac{e}{\gamma_o m_o \Omega_n} \left[- \frac{B_w}{2c} \left(v_{yn-1} + v_{yn+1} \right) + i \frac{v_2}{2c} \left(B_{xn-1} - B_{xn+1} \right) + \right.$$

$$\left. i \frac{v_o v_2}{2c^2} \left(E_{yn-1} - E_{yn+1} \right) + \frac{1}{\gamma_o^2} E_{\ell n} \right]$$

where

$$\Omega_n = \omega - v_o k_n . \qquad (15)$$

From the Maxwell equation $\nabla \times \vec{E} + (1/c) \partial \vec{B} / \partial t = 0$ we have, $B_{xn} = -(ck_n/\omega) E_{yn}$. Neglecting small quantities, Eq. (14) simplifies as follows:

$$v_{xn} = - i \frac{\Omega_{\parallel}}{\Omega_n} v_{yn}$$

$$v_{yn} = i \frac{\Omega_{\parallel}}{\Omega_n} v_{xn} - i \frac{e}{\gamma_o m_o \omega} E_{yn} \qquad (16)$$

$$v_{zn} = - i \frac{e}{\gamma_o^3 m_o \Omega_n} E_{\ell n} + i \frac{1}{2} \frac{\Omega_w}{\Omega_n} \left(v_{yn-1} + v_{yn+1} \right) + \frac{e v_2}{2 \gamma_o m_o \omega \Omega_n} \left[\left(\frac{v_o \omega}{c^2} - k_{n-1} \right) E_{yn-1} - \right.$$

$$\left. \left(\frac{v_o \omega}{c^2} - k_{n+1} \right) E_{yn+1} \right] .$$

Solving for the velocity components, Eqs. (16) then become

$$v_{xn} = - \frac{\Omega_{\parallel}/\Omega_n}{1 - \left(\Omega_{\parallel}/\Omega_n \right)^2} \frac{e}{\gamma_o m_o \omega} E_{yn}$$

$$v_{yn} = - i \frac{1}{1 - \left(\Omega_{\parallel}/\Omega_n \right)^2} \frac{e}{\gamma_o m_o \omega} E_{yn} \qquad (17)$$

$$v_{zn} = - i \frac{e}{\gamma_o^3 m_o \Omega_n} E_{\ell n} + \frac{1}{2} \frac{\Omega_w}{\omega} \frac{e}{\gamma_o m_o} \left[\frac{1}{1 - (\Omega_{\parallel}/\Omega_{n-1})^2} \frac{1}{\Omega_n} E_{yn-1} + \frac{1}{1 - (\Omega_{\parallel}/\Omega_{n+1})^2} \frac{1}{\Omega_n} E_{yn+1} \right] +$$

$$+ \frac{e v_2}{2\gamma_o m_o \omega \Omega_n} \left[\left(\frac{v_o \omega}{c^2} - k_{n-1} \right) E_{yn-1} - \left(\frac{v_o \omega}{c^2} - k_{n+1} \right) E_{yn+1} \right] .$$

The linearized current density $J=-e(n\vec{v}^0+n_o\vec{v})$ is obtained from Eqs. (8) and (10) with the result that,

$$j_{xn} = - e n_o v_{xn} - e n_o \frac{v_1}{2} \left(\frac{k_{n-1} v_{zn-1}}{\Omega_{n-1}} + \frac{k_{n+1} v_{zn+1}}{\Omega_{n+1}} \right)$$

$$j_{yn} = - e n_o v_{yn} + i e n_o \frac{v_2}{2} \left(\frac{k_{n-1} v_{zn-1}}{\Omega_{n-1}} - \frac{k_{n+1} v_{zn+1}}{\Omega_{n+1}} \right) \qquad (18)$$

$$j_{zn} = - e n_o \frac{\omega}{\Omega_n} v_{zn} \quad .$$

Inserting Eqs. (17) and (18) in the wave Eq. (9) yields the dispersion relation,

$$\omega^2 - c^2 k_n^2 - \frac{\omega_p^2 \Omega_n^2}{\Omega_n^2 - \Omega_{\parallel}^2} = \frac{\gamma_o^2 \Omega_{n-1}^2}{\gamma_o^2 \Omega_{n-1}^2 - \omega_p^2 \gamma_o^2} \frac{\omega_p^4}{4} \frac{v_2}{} \left[\frac{\Omega_w \Omega_n^2}{\Omega_n^2 - \Omega_{\parallel}^2} - \right.$$

$$\left. - v_2 \left(\frac{v_o}{c^2} \omega - k_n \right) \right] \frac{k_{n-1}}{\Omega_{n-1}^4} - \frac{\gamma_o^2 \Omega_{n+1}^2}{\gamma_o^2 \Omega_{n+1}^2 - \omega_p^2 \gamma_o^2} \frac{\omega_p^4}{4} \frac{v_2}{} \left[\frac{\Omega_w \Omega_n^2}{\Omega_n^2 - \Omega_{\parallel}^2} + \right. \qquad (19)$$

$$\left. + v_2 \left(\frac{v_o}{c^2} \omega - k_n \right) \right] \frac{k_{n+1}}{\Omega_{n+1}^4}$$

where $\omega_p=(4\pi n_o e^2/m_o\gamma_o)^{\frac{1}{2}}$ is the plasma frequency. We are interested only in the lowest mode, n=0 and upshifted frequencies $\omega\simeq(k+k_w)v_o$. In this case Eq. (19) reduces to the sought-after dispersion equation,

$$\left[\omega^2 - c^2k^2 - \frac{\omega_p^2(\omega - v_o k)^2}{(\omega - v_o k)^2 - \Omega_{\parallel}^2}\right]\left\{\left[\omega - v_o(k + k_w)\right]^2 - \frac{\omega_p^2}{\gamma_o^2}\right\} \tag{20}$$

$$= -\frac{\omega_p^2}{4}\frac{\Omega_w^2 v_o^2 k_w}{\Omega_{\parallel}^2 - v_o^2 k_w^2}\left[\frac{(\omega - v_o k)^2}{(\omega - v_o k)^2 - \Omega_{\parallel}^2} + \frac{v_o^2 k_w}{\Omega_{\parallel}^2 - v_o^2 k_w^2}\left(\frac{v_o}{c^2}\omega - k\right)\right](k + k_w)$$

This sixth order equation in ω has been solved on a computer for real k and complex ω, and detailed results will be discussed in section IV. However, when one makes the approximations $\omega \simeq ck$, $\omega \simeq (k+k_w)v_o$, one finds the following results for the real and imaginary parts of the complex frequency:

$$\omega_r \simeq (1 + \beta_o)\gamma_o^2 k_w c\beta_o \tag{21a}$$

$$\omega_i \simeq \frac{\Omega_{wo}}{4\gamma_o^{3/4}|1 - R^2|}\left[\left(\frac{\omega_{po}}{k_w c}\right)\left(\frac{1 + \beta_o}{\beta_o}\right)\right]^{\frac{1}{2}} . \tag{21b}$$

Here ω_r is the approximate radiation frequency at maximum growth rate, ω_i, of the FEL instability; $\Omega_{wo}=eB_w/m_o c$ and $\Omega_{\parallel o}=eB_{\parallel}/m_o c$ are now the nonrelativistic electron cyclotron frequencies in the wiggler and guide fields respectively; $\omega_{po}=(4\pi ne^2/m_o)^{\frac{1}{2}}$ is the nonrelativistic plasma frequency; and $R=(\Omega_{\parallel o}/\gamma_o k_w c\beta_o)$. We see that the real part of the frequency exhibits the familiar γ_o^2 upshift and that the imaginary part exhibits the familiar resonance[6] at R=1. We point out, however, that our result is only applicable when inequality (4) is satisfied, so that R must not be too close to unity.

2. TEM Mode of Polarization

For the TEM mode of polarization, the RF field components are $\vec{E}=\hat{x}E_x$ and $\vec{B}=\hat{y}B_y$. Proceeding the same way as we did in the above section, we obtain the following expression for the dispersion equation:

$$\left[\omega^2 - c^2k^2 - \frac{\omega_p^2(\omega - v_o k)^2}{(\omega - v_o k)^2 - \Omega_{\shortparallel}^2}\right]\left\{\left[\omega - v_o(k + k_w)\right]^2 - \frac{\omega_p^2}{\gamma_o^2}\right\} \tag{22}$$

$$= -\frac{\omega_p^2}{4}\,\frac{\Omega_w^2\Omega_{\shortparallel}^2 v_o}{\Omega_{\shortparallel}^2 - v_o^2k_w^2}\left[\frac{\omega - v_o k}{(\omega - v_o k)^2 - \Omega_{\shortparallel}^2} - \frac{v_o k}{\Omega_{\shortparallel}^2 - v_o^2k_w^2}\right](k + k_w)$$

Detailed solutions of this equation for real k and complex ω are presented in section IV. An approximate result subject to the assumptions $\omega \simeq ck$, $\omega \simeq (k+k_o)v_o$ is

$$\omega_r \simeq (1 + \beta_o)\gamma_o^2 k_w c\beta_o \tag{23a}$$

$$\omega_i \simeq \frac{\Omega_{wo}\Omega_{\shortparallel o}}{4\gamma_o^{3/4}|1 - R^2|}\left[\frac{\omega_{po}}{(k_w c)^3}\left(\frac{1 + \beta_o}{\beta_o^3}\right)\right]^{\frac{1}{2}} \tag{23b}$$

Comparison of Eq. (23b) with Eq. (21b) shows that whereas the growth rate of the TE mode varies as B_w, that of the TEM mode varies as the product $B_w B_{\shortparallel}$ and is zero in the absence of the guide magnetic field. This is readily understood. When $B_{\shortparallel}$ is zero, the oscillatory $-e\vec{v}_o \times \vec{B}_w \cos(k_w z)$ force is in the y direction (see Fig. 1) and the RF electric field of the electromagnetic wave is therefore also polarized totally in the y direction. When $B_{\shortparallel}$ is finite, the helical motion of the electrons in the guide field is coupled to the y-directed quiver motion in the wiggler field. Hence, the RF electric field acquires a component in the x direction and thus excites a TEM mode. This is of considerable practical interest since the TEM mode has no low frequency cutoff, and the waveguide walls can be brought (arbitrarily) close together. This allows one to bring the wiggler magnets close together, increase B_w and thus increase the instability growth rate. We note that the same reasoning used for the parallel plate waveguide also applies to the lowest mode of a rectangular waveguide that would be used in practice.

IV. RESULTS AND DISCUSSION

The FEL instability discussed in the previous section comes about as a result of the coupling of the negative energy space charge wave on the electron beam

$$\omega = (k + k_w)v_o - (\omega_p/\gamma_o) \tag{24}$$

and the linearly polarized electromagnetic wave,

$$k^2c^2 = \omega^2 - \frac{\omega_p^2(\omega - kv_o)^2}{(\omega - kv_o)^2 - \Omega_{\parallel}^2} . \tag{25}$$

This is readily seen by setting the coupling term on the right-hand side of Eqs. (20) and (22) equal to zero. There are two unstable waves, one at high frequency which is of primary interest and whose frequency is approximately given by Eqs. (21a) or (23a), and one at low frequency. The high frequency wave propagates along the positive z axis and is associated with positive wave numbers k. The low frequency wave propagates along the negative z axis in the absence of a guiding magnetic field (k<0). However, if $B_{\parallel}$ is sufficiently large, k for this wave can also be positive.[23] This happens when

$$\left[\left(k_w v_o - \frac{\omega_p}{\gamma_o}\right)^2 - \omega_p^2\right]^{\frac{1}{2}} < \Omega_{\parallel} < \left[\left(k_w v_o - \frac{\omega_p}{\gamma_o}\right)^2 - \frac{\omega_p^2}{\gamma_o^2}\right]^{\frac{1}{2}} \tag{26}$$

a result which is obtained by eliminating ω from Eqs. (24) and (25) and solving for k.

The dispersion characteristics (ω_i versus k) are illustrated in Fig. 5 for a high voltage, high current beam for which V=1.275MV, J=4.3kA/cm^2; γ_o=3.50; ω_p =2.93×10^{10}sec^{-1}; $B_{\parallel}$=9.8kG, B_w=0.4kG, ℓ=3cm (k_w=2.09cm^{-1}). They were computed by solving Eqs. (20) and (22) on a computer. The TE and TEM modes each exhibit two maxima corresponding to the low and high frequency waves discussed above. Their dispersion characteristics are seen to overlap. Both waves propagate in

the positive z direction since inequality (26) is satisfied (the smallest value of $B_{\parallel}$ given by Eq. (26) is 8.84kG, for the above values of k_w, v_o and ω_p). The maximum growth rates shown in Fig. 5 for the high frequency TE and TEM modes agree very well with those obtained from the approximate Eqs. (21b) and (23b), respectively.

Growth rate curves like those shown in Fig. 5 have been obtained for a number of guide magnetic fields $B_{\parallel}$, with all other parameters held constant. The respective maximum growth rates are illustrated in Fig. 6. We note that at low magnetic fields the growth rate of the TE mode is larger than that of the TEM mode, but the situation reverses at higher magnetic fields. Resonance occurs when $R \equiv (\Omega_{\parallel}/k_w v_o) \approx 1$ which corresponds to $B_{\parallel}$=12kG. However, near this resonance our calculations become inapplicable and are not shown; only those results are graphed for which inequality (4) is well-satisfied. Figure 7 shows the corresponding real parts of the dispersion characteristics, namely ω_r, and the phase velocity $v_p=\omega_r/k$, as a function of $B_{\parallel}$. We see that for magnetic fields above the resonance, both waves are subluminous $(v_p<c)$, but below the resonance the TE wave is superluminous but the TEM wave subluminous.

The remainder of this section is devoted to free electron laser operation using almost nonrelativistic,[18] low current beams with 300kV, 160A/cm^2 and 30kV, 22.3A/cm^2, respectively. The 300kV, 160A/cm^2 results are qualitatively similar to those shown in Figs. 5 through 7 and are not graphed. Instead, the results are summarized in Table 2.

For the 30kV, 22.3A/cm^2 beam[24] we have γ_o=1.059, $\omega_p=6.52\times10^9 sec^{-1}$; we also take $B_{\parallel}$=1kG, B_w=0.2kG, ℓ=2cm (k_w=3.14cm^{-1}). The imaginary part of the dispersion characteristic is shown plotted in Fig. 8. For the magnetic field $B_{\parallel}$ which we have chosen, inequality (26) is not satisfied, and therefore there are only two high frequency waves (TE and TEM) with positive k, rather than the four waves shown in Fig. 5. Figure 9 illustrates how the maximum growth rate varies

with the axial guide magnetic field $B_{\parallel}$, with all remaining parameters being fixed at their previously stated values. The resonance $R\equiv(\Omega_{\parallel}/k_w v_o)=1$ occurs at $B_{\parallel}=1.86$ kG. We knote that for low velocity but fairly high density beams such that $k_w v_o$ is comparable with ω_p/γ_o, the radiation frequency is considerably less than that given by the familiar result, $\omega_r=(1+\beta_o)\gamma_o^2 k_w v_o$ (Eqs. (21a), (23a)). Solving Eqs. (24) and (25) yields a more accurate value of the radiation frequency (in the limit of weak coupling, $\Omega_w \to 0$):

$$\omega_r = \left(k_w v_o - \frac{\omega_p}{\gamma_o}\right)\gamma_o^2\left[1 + \beta\left\{1 - \frac{\omega_p^2}{(\gamma_o k_w v_o - \omega_p)^2 - \gamma_o^2\Omega_{\parallel}^2}\right\}^{\frac{1}{2}}\right], \qquad (k_w v_o > \omega_p/\gamma_o) \quad (27)$$

For a cold, dense electron beam, the growth rate ω_i of the FEL instability increases almost linearly with increasing wiggler magnetic field B_w (cf Eqs. (21b), (23b). However, when B_w is very large (or ω_p is correspondingly small) departures from linearity become more and more pronounced. Here the electron susceptibility $\omega_p^2\gamma_o^{-2}(\omega-kv_o)^{-2}$ approaches zero, the collective bunching force becomes small relative to the ponderomotive force and one enters[1,2] the single particle, noncollective, high-gain FEL region of operation. This is illustrated in Fig. 11 where we see departures from linearity at the higher values of B_w. To observe this, we purposely reduced the value of ω_p from that used in an earlier example (see Table 2).

In calculating the growth rate, we have assumed implicitly that the parallel-plate waveguide is filled uniformly with electrons. In practice, the cross sectional area of the beam is not uniform and the beam does not fill the waveguide. To obtain a more realistic growth rate, the values given should be multiplied by a semiempirical factor[2] $f^{\frac{1}{4}}$ where f is the ratio of the cross sectional area of the electron beam to the cross sectional area of the waveguide.

In order for the electromagnetic wave to grow, the electron velocity v_o must be slightly larger than the phase velocity of the space charge wave v_s. As

the electrons lose energy to the wave, the difference $v_o - v_s$ becomes zero and growth ceases. This represents a nonlinear saturation which limits the maximum achievable efficiency η of the free electron laser. Its value can be estimated from the expression[1]

$$\eta \approx \frac{\Delta\varepsilon}{m_o c^2 (\gamma_o - 1)} \tag{28}$$

where $\Delta\varepsilon$ is the change in kinetic energy at saturation when the particles are deeply trapped. Computing $\Delta\varepsilon$ yields

$$\eta = -\left(\frac{2\beta_o \gamma_o^3}{\gamma_o - 1}\right)\left(\beta_o - \frac{\omega_r}{c(k + k_w)}\right) \tag{29}$$

where ω_r and k are obtained from solving dispersion Eqs. (20) and (22). The computed efficiencies are listed in Table 1.

In conclusion, we have discussed the real and imaginary components of the free electron laser dispersion equations for the case of a cold electron beam propagating in a parallel-plate waveguide and subjected simultaneously to a linearly polarized wiggler magnetic field, and an axial guide magnetic field. We have computed the growth rates of the FEL instability for two modes of polarization of the electromagnetic wave. One in which the RF electric field is polarized at right angles to the wiggler magnetic field (TE waveguide mode), and the other in which the electric field is polarized along the direction of the wiggler field (TEM mode). At sufficiently high guide magnetic fields the parallel-polarized (TEM) component can dominate the conventional cross-polarized (TE) mode. These effects have not been examined previously in a detailed manner and are directly relevant to ongoing experiments.[22,24]

Calculations show that the effects of the $\vec{B}\times\nabla\vec{B}/|\vec{B}|^2$ drift inherent in a system comprised of a linearly polarized wiggler and guide magnetic field may

not be too damaging to the operation of the FEL. An electron injected into the wiggler exactly on axis $x_o=y_o=0$ exhibits no net drift, and electrons that are almost paraxial exhibit but small drifts. Thus, a pencil beam of small radius will propagate down the wiggler with relatively little deviation, as is illustrated in Figs. 3 and 4.

At low voltages, free electron lasers exhibits good efficiencies and growth rates even for beams with moderate currents (see Table 1). Their performance compares very favorably with that of gyrotrons.[25] We have also seen that the application of an axial guide magnetic field increases the linear growth rate of the FEL instability even when the magnetic field is quite far from the resonant condition, $R=\Omega_{\parallel}/k_w v_o \simeq 1$. This aspect of the problem has not been exploited in the UBITRON[18] which was operated without a guide field.

ACKNOWLEDGMENTS

This work was supported in part by the Department of the Air Force Aeronautical Systems Division (AFSC), in part by the Air Force Office of Scientific Research, and in part by the National Science Foundation.

REFERENCES

1. P.A. Sprangle, R.A. Smith, and V.L. Granatstein in "Infrared and Submillimeter Waves", K. Button editor (Academic Press N.Y. 1979) Vol. 1 p. 279 and references therein; also P.A. Sprangle and R.A. Smith, Phys. Rev. A21, 293 (1980).

2. N.M. Kroll and W. A. McMullin, Phys. Rev. A17, 300 (1978).

3. P.A. Sprangle, Cha-Mei Tang and W. M. Manheimer, Phys. Rev. A21, 302 (1980).

4. R.C. Davidson and H.S. Uhm, Phys. Fluids 23, 2076 (1980).

5. T. Kwan, J.M. Dawson, and A.T. Lin, Phys. Fluids 20, 581 (1977).

6. B.M. Kincaid, J. Appl. Phys. 48, 2684 (1977); also J.P. Blewett and R. Chasman, J. Appl. Phys. 48, 2692 (1977).

7. J.M. Buzzi, K. Feld, and L. Vallier, Laboratoire de Physique des Milieux Ionises, Ecole Polytechnique Palaiseau France Report No. PMI 1008 (1980).

8. Cha-Mei Tang and P.A. Sprangle, J. Apply Phys. 52, 3148 (1981).

9. D. Prosnitz, A. Szoke, and V.K. Neil, Phys. Rev. A24 1436 (1981).

10. Ren-Chau J. Hu, L.R. Elias, University of California, Santa Barbara, Quantum Institute Report No. QIFEL019/83 (1983).

11. C.W. Roberson, J. A. Pasour, F. Mako, R. Lucey, and P.A. Sprangle, Naval Research Laboratory, Washington, DC, Memorandum Report No. 5013 (1983).

12. K. Halbach, Lawrence Berkeley Laboratory, University of California Accelerator and Fusion Research Division Report No.LBL11393, August 1980.

13. K. Halbach, J. Chin, E. Hoyer, H. Winick, R. Cronin, J. Yang, Y. Zambre, Proceedings of the 1981 Particle Accelerator Conference March 11-13, Washington, DC

14. R.C. Davidson "Theory of Nonneutral Plasmas" (W.A. Benjamin 1974)

15. L. Friedland, Phys. Fluids 23, 2376 (1980).

16. H.P. Freund and P. Sprangle, Phys. Rev. A24, 1965 (1981).

17. W. A. McMullin and R.C. Davidson, Phys. Rev. A25, 3130 (1982); also, I.B. Bernstein and L. Friedland, Phys. Rev. A23, 816, (1981); L. Friedland and A. Fruchtman, Phys. Rev. A25, 2693 (1982).

18. R.M. Phillips, IRE Trans, Electron Devices, p. 231, Oct. 1960.

19. R.E. Shefer and G. Bekefi, Appl. Phys. Lett. 37, 901 (1980).

20. R.H. Jackson, S.H. Gold, R.K. Parker, H.P. Freund, P.C. Efthimion, V.L. Granatstein, M. Herndon, A.K. Kinkead, J.E. Kosakowski, and T.J.T. Kwan, IEEE J. Quant. Electronics QE-19, 346 (1983).

21. G. Hall and J.M. Watt, editors, "Modern Numerical Methods for Ordinary Differential Equations" (Clarendon Press, Oxford, 1976).

22. J.A. Pasour, F. Mako, and C.W. Roberson, J. Appl. Phys. 53, 7174 (1982).

23. A.T. Lin, Chih Chien Lin, T. Taguchi, and W.W. Cheng, Phys. Fluids 26, 3 (1983).

24. K.D. Jacobs and G. Bekefi, Bull. Am. Phys. Soc. 27, 1010 (1982).

25. J.L. Hirshfield and V.L. Granatstein, Comments Plasma Phys. Cont. Fusion 3, 87 (1977) and references therein.

CAPTIONS TO FIGURES

Fig. 1. (a) Schematic of an electron beam in a linearly polarized wiggler generated by a periodic system of bar magnets. (b) Practical version of the wiggler showing computer generated magnetic field lines.

Fig. 2. (a) Projection onto the x-y plane of the electron displacements after traversing a distance z=15.5cm. Initial positions $x_o=y_o=0$ at z=0. (b) Radial displacement $r=(x^2+y^2)^{\frac{1}{2}}$ as a function of the axial position z. V=300kV; $B_{\parallel}$=5kG; B_w=0.5kG; ℓ=1.0cm.

Fig. 3. Same as Fig. 2 except that initially the electron is positioned off axis with x_o=0.1cm, y_o=0 at z=0; electron drift occurs along -y direction. In (b) are shown only the maxima and minima of the electron displacements.

Fig. 4. Electron drift plus oscillatory displacement y_{max} as a function of the strength of (a) the wiggler field and (b) the guide magnetic field after traversing a distance z≃100cm. V=300kV; ℓ=1cm; x_o=0.1cm; y_o=0.

Fig. 5. Normalized growth rate of the FEL instabilities as a function of the normalized wave number for two modes of polarization of the electromagnetic wave. V=1.275MV; J=4.3kA/cm^2; $\omega_p=2.93\times10^{10}sec^{-1}$; $B_{\parallel}$=9.8kG; B_w=0.4kG, ℓ=3cm.

Fig. 6. Normalized growth rate as a function of the guide magnetic field. The dashed line corresponds to the resonance $R=\Omega_{\parallel}/k_w v_o=1$. V=1.275MV; J=4.3kA/cm^2; $\omega_p=2.93\times10^{10}sec^{-1}$, B_w=0.4kG, ℓ=3cm.

Fig. 7. Frequency and phase velocities of the TE and TEM modes as a function of the axial guide magnetic field. V=1.275MV; J=4.3kA/cm^2; ω_p = $2.93\times10^{10}sec^{-1}$; B_w=0.4kG; ℓ=3cm.

Fig. 8. Real and imaginary parts of the frequency as a function of the wave number for two modes of polarization. The curves for the real parts

of the two modes are too close to one another to be distinguishable $V=30kV$; $J=22.3A/cm^2$; $\omega_p=6.52\times10^9sec^{-1}$; $B_{\parallel}=1kG$; $B_w=0.2kG$; $\ell=2cm$.

Fig. 9. Normalized growth rate as a function of the axial guide magnetic field for two modes of polarization. The dashed portions of the curves correspond to regions where inequality (4) is not well-satisfied. $V=30$ kV; $J=22.3A/cm^2$; $\omega_p=6.52\times10^9sec^{-1}$; $B_w=0.2kG$; $\ell=2cm$.

Fig. 10. Frequency and phase velocity as a function of the axial guide magnetic field. The dashed portions of the curves correspond to regions where inequality (4) is not well-satisfied. The curve for the TE and TEM modes are too close to be distinguished from one another. $V=30kV$; $J=22.3A/cm^2$; $\omega_p=6.52\times10^9sec^{-1}$; $B_w=0.2kG$; $\ell=2cm$.

Fig. 11. Growth rate as a function of the strength of the wiggler magnetic field, showing departures from linearity (dashed straight lines). $V=300kV$; $J=16A/cm^2$; $\omega_p=2.92\times10^9sec^{-1}$; $B_{\parallel}=5kG$; $\ell=1cm$.

Table 1. Summary of FEL parameters

Beam voltage (kV)	30	300	1275
Beam current density (Acm^{-2})	22.3	160	4300
Axial magnetic field (kG)	1.0	5.0	5.5
Wiggler field (kG)	0.20	0.50	0.55
Period of wiggler (cm)	2.0	1.0	3.0
Radiation wavelength (cm)	5.17	0.30	0.15
Spatial growth rate of TE mode (dB/m)	20.0	19.7	45.7
Spatial growth rate of TEM mode (dB/m)	12.2	11.8	69.1
Efficiency TE mode (%)	63	7.6	21
Efficiency TEM mode (%)	63	7.6	21

Table 2. FEL parameters for a 300kV, 160A/cm^2 beam; γ_o=1.59; ω_p=9.25×10^{9}sec^{-1}; $B_{\parallel}$=5kG; B_w=0.5kG; ℓ=1cm (k_w=6.28cm^{-1}).

PARAMETER	TE MODE	TEM MODE
ω_i/ω_p	0.074	0.044
ω_r/ω_p	68.1	68.1
v_p/c	1.00010	1.00012

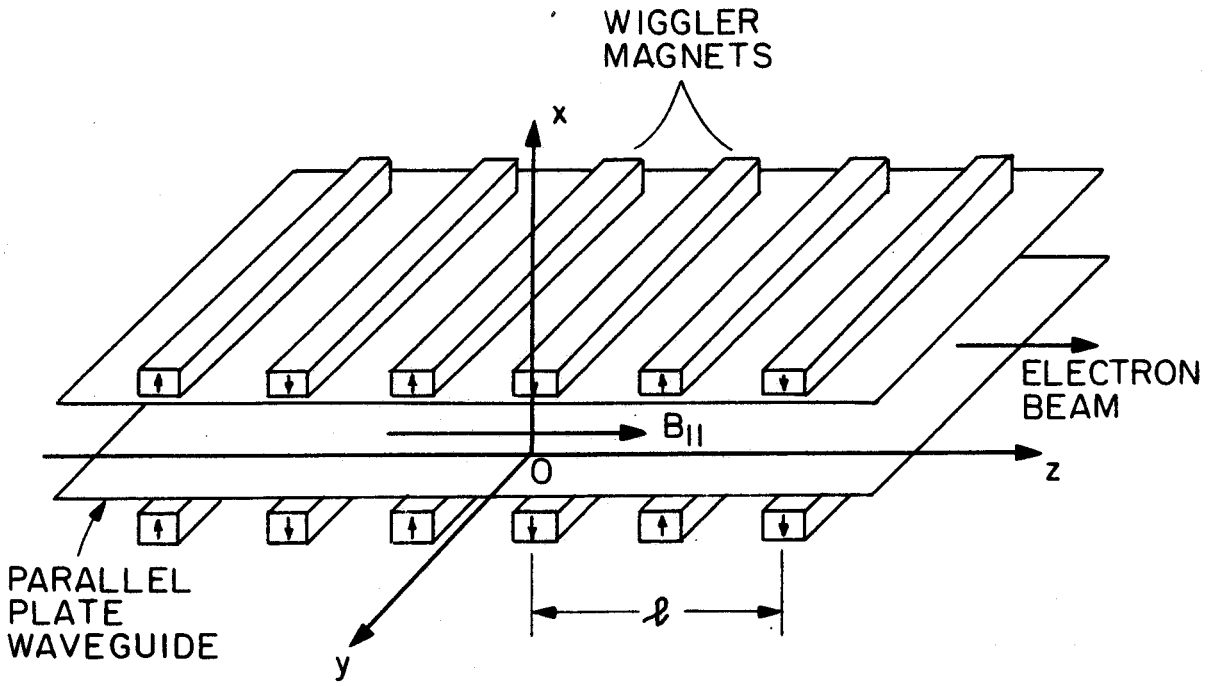

(a)

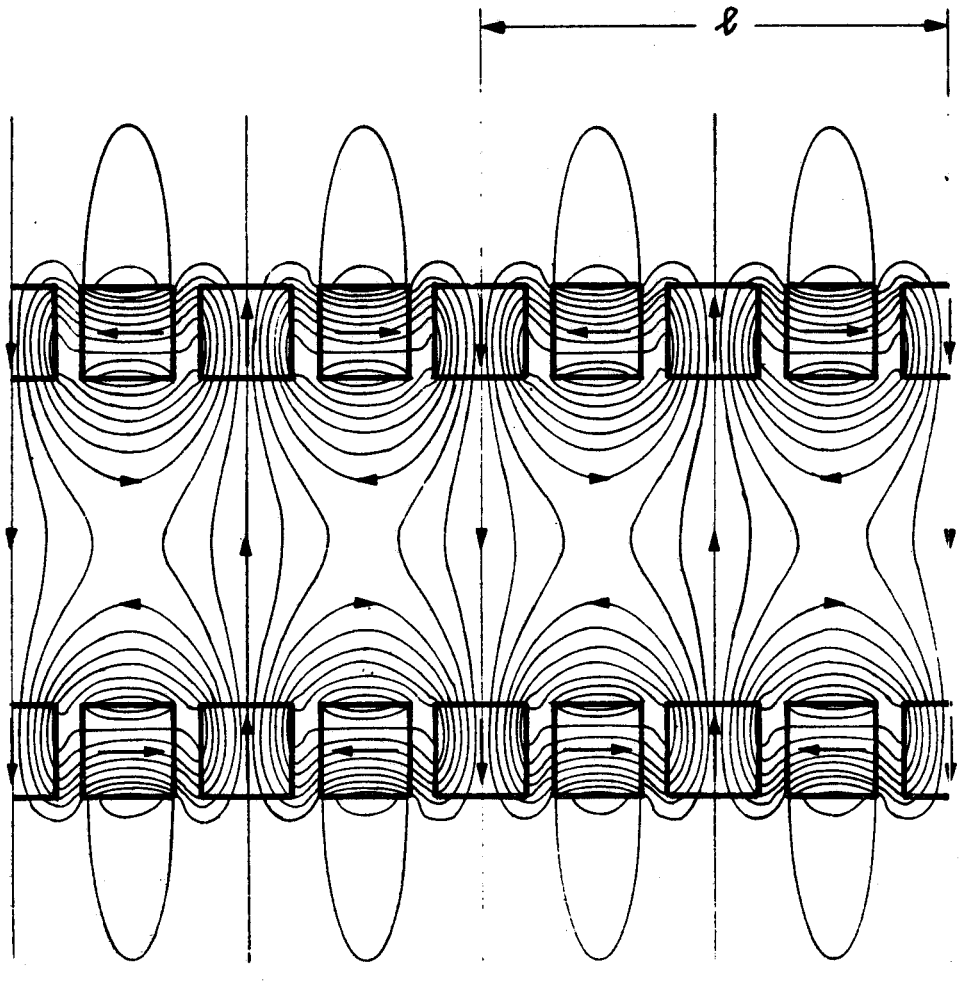

(b)

Fig. 1
Yin, Bekefi

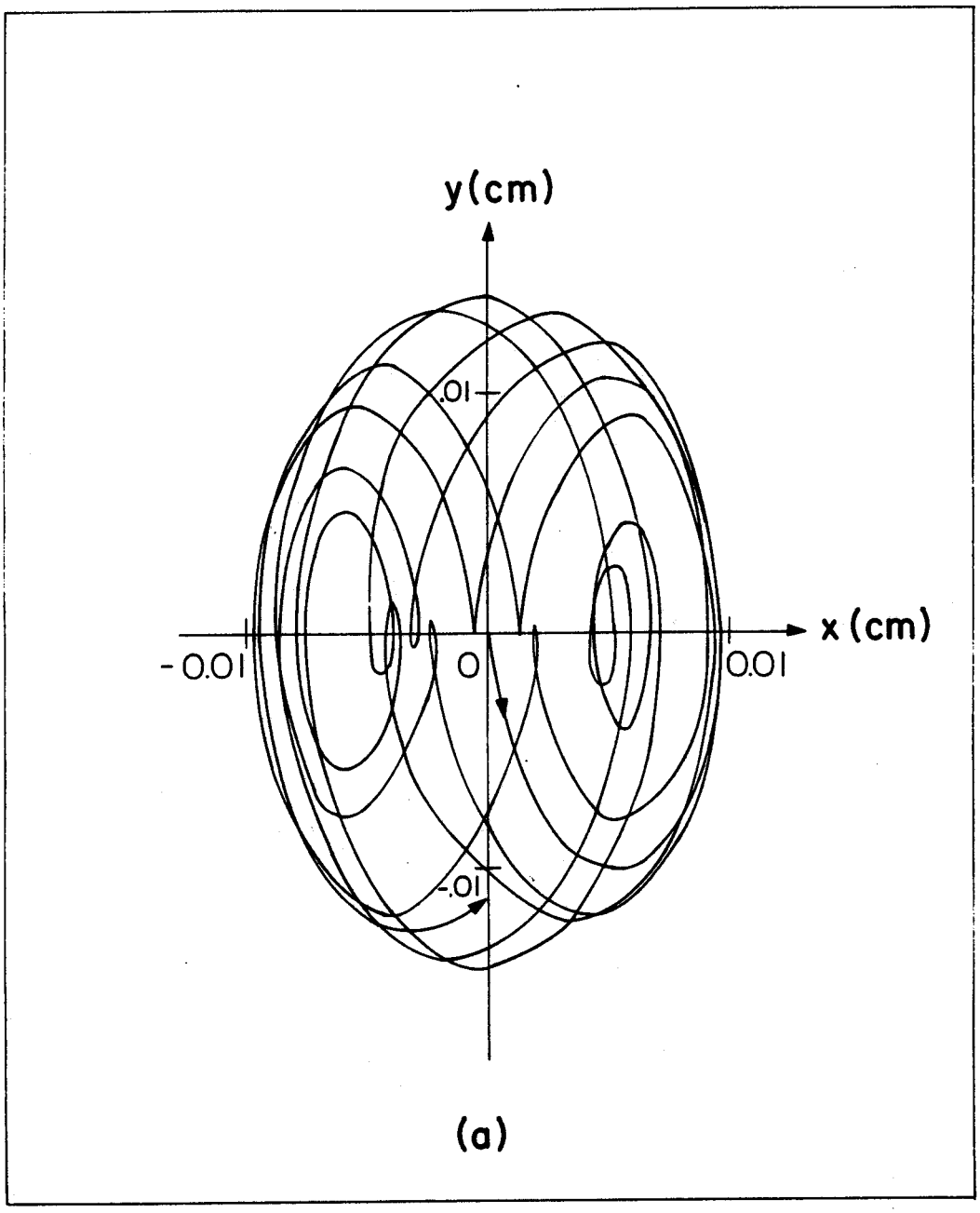

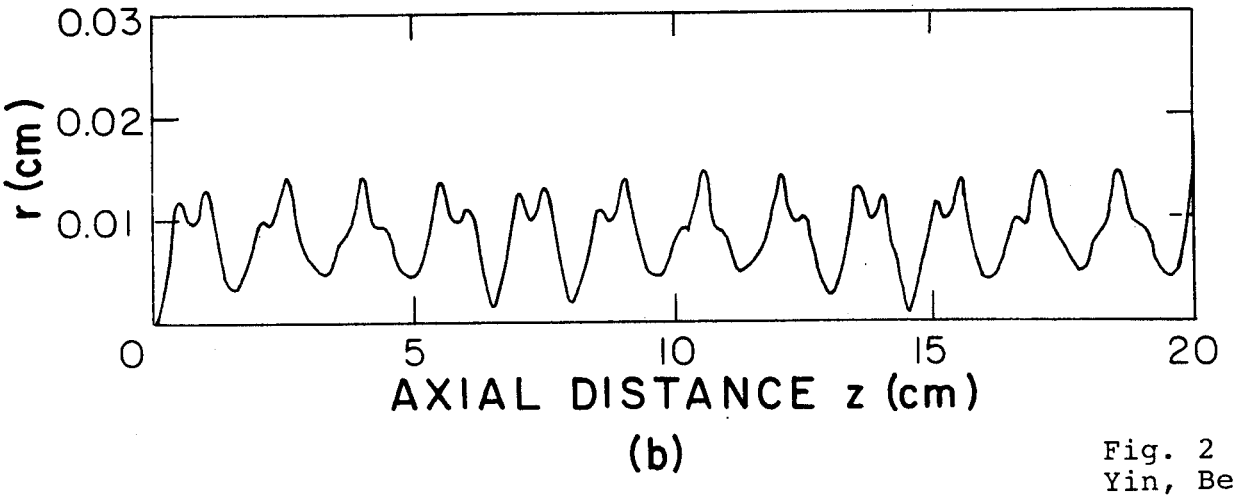

Fig. 2
Yin, Bekefi

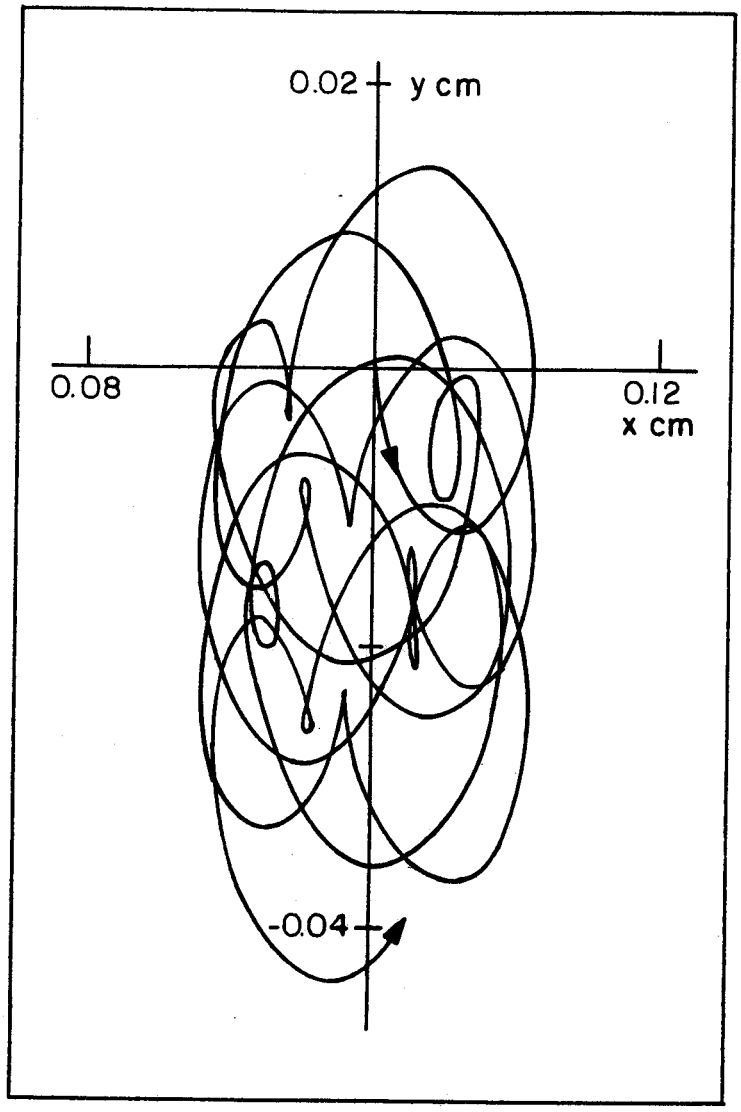

(a)

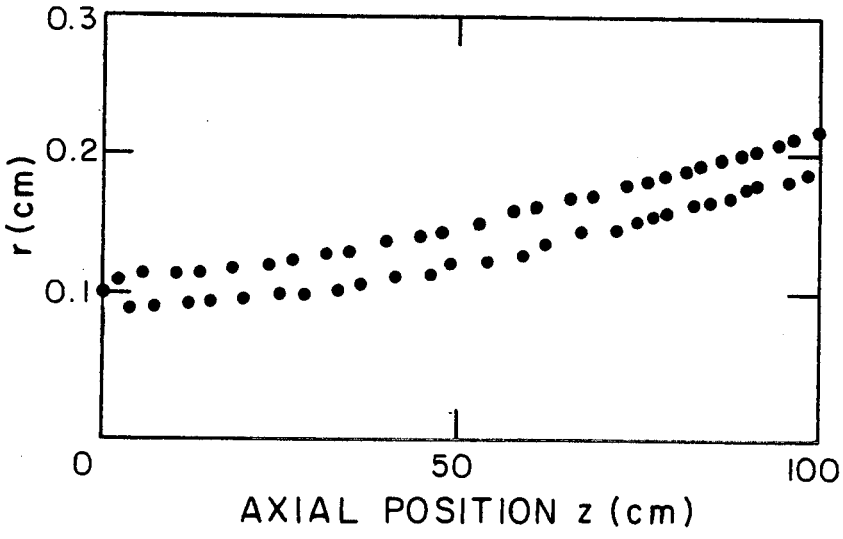

(b)

Fig. 3
Yin, Bekefi

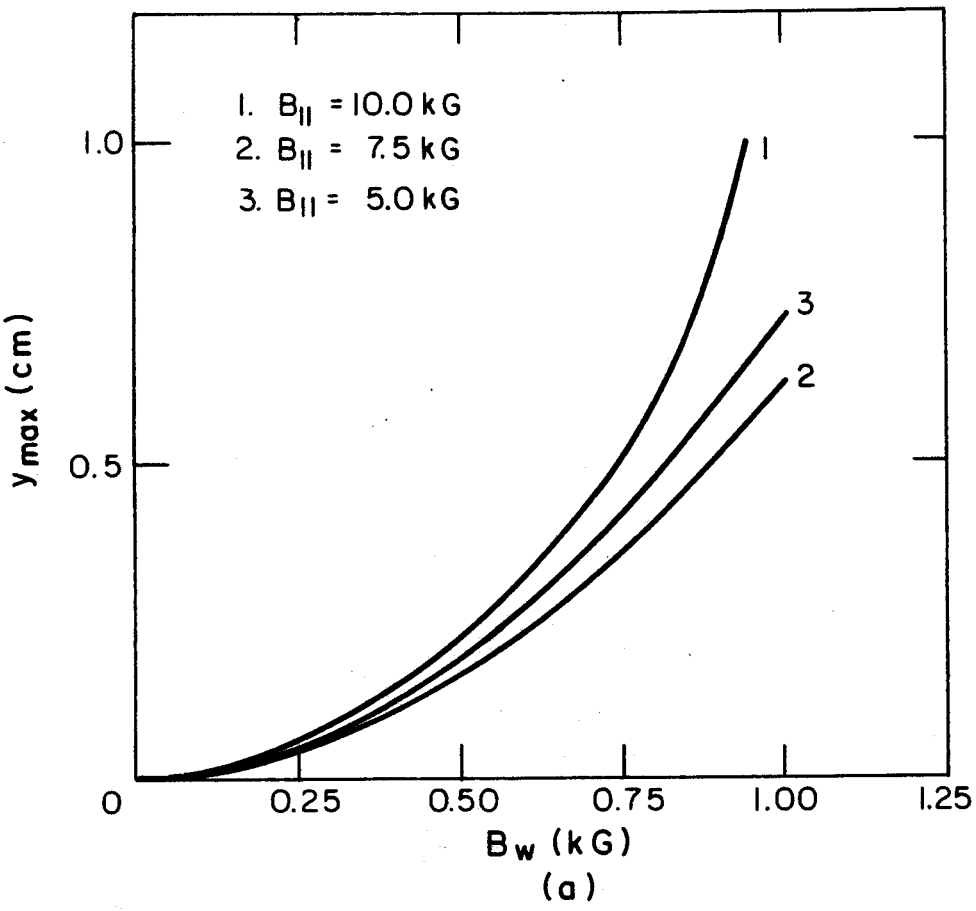

(a)

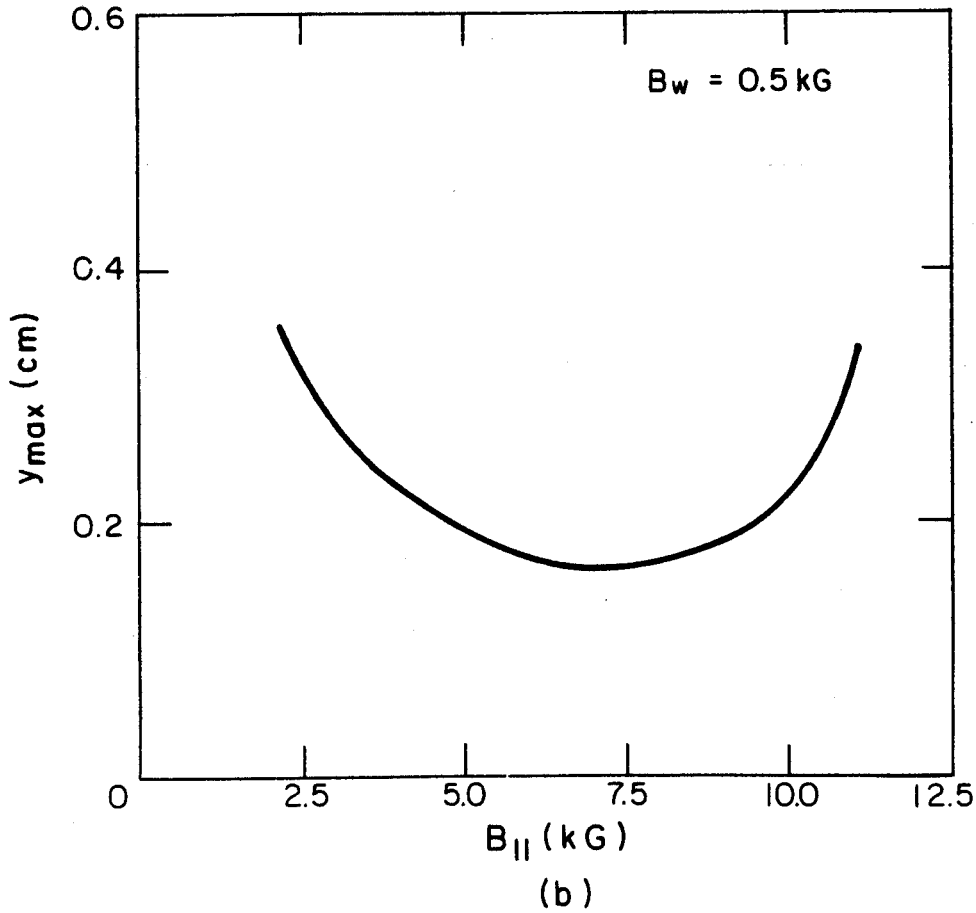

(b)

Fig. 4
Yin, Bekefi

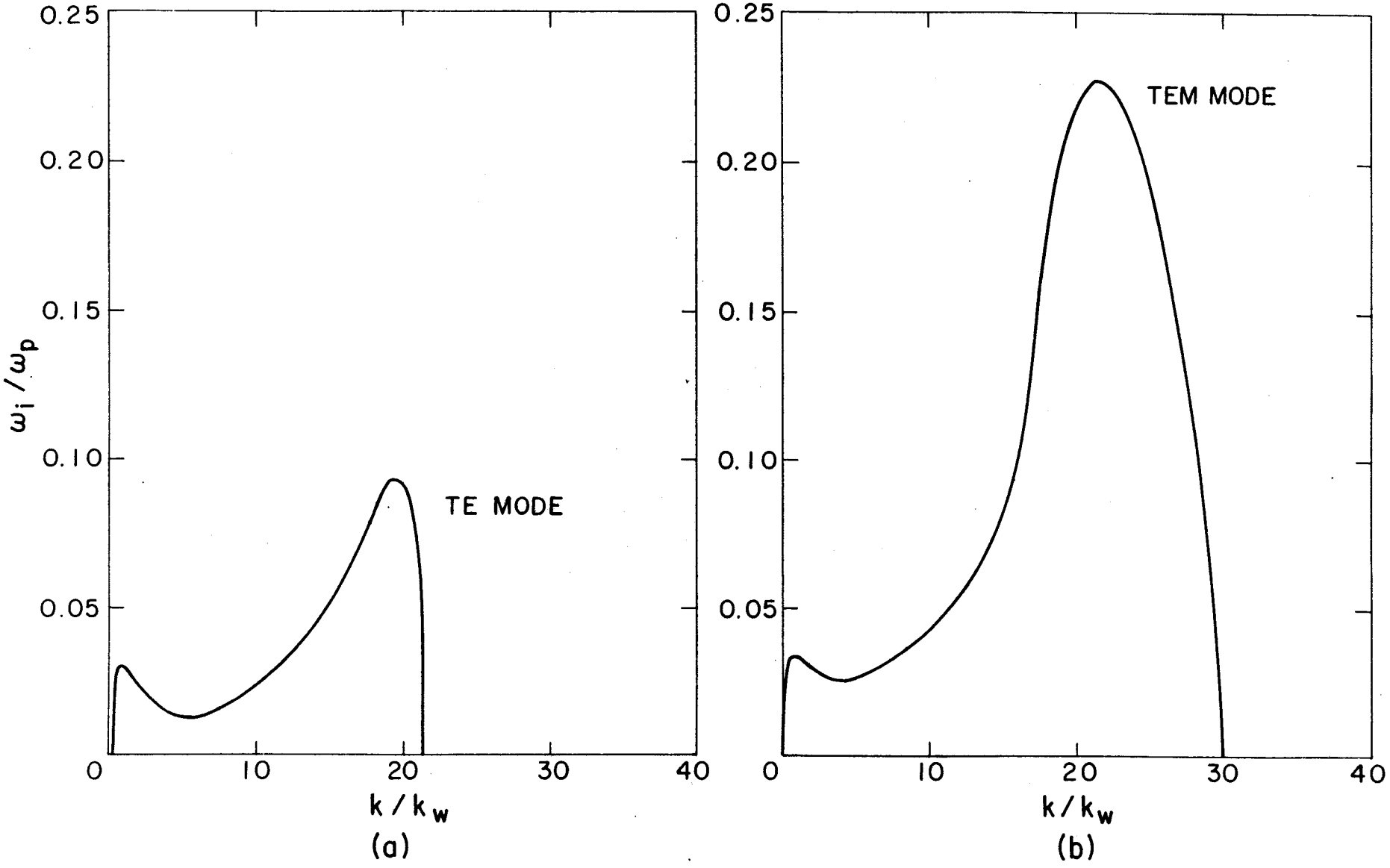

Fig. 5
Yin, Bekefi

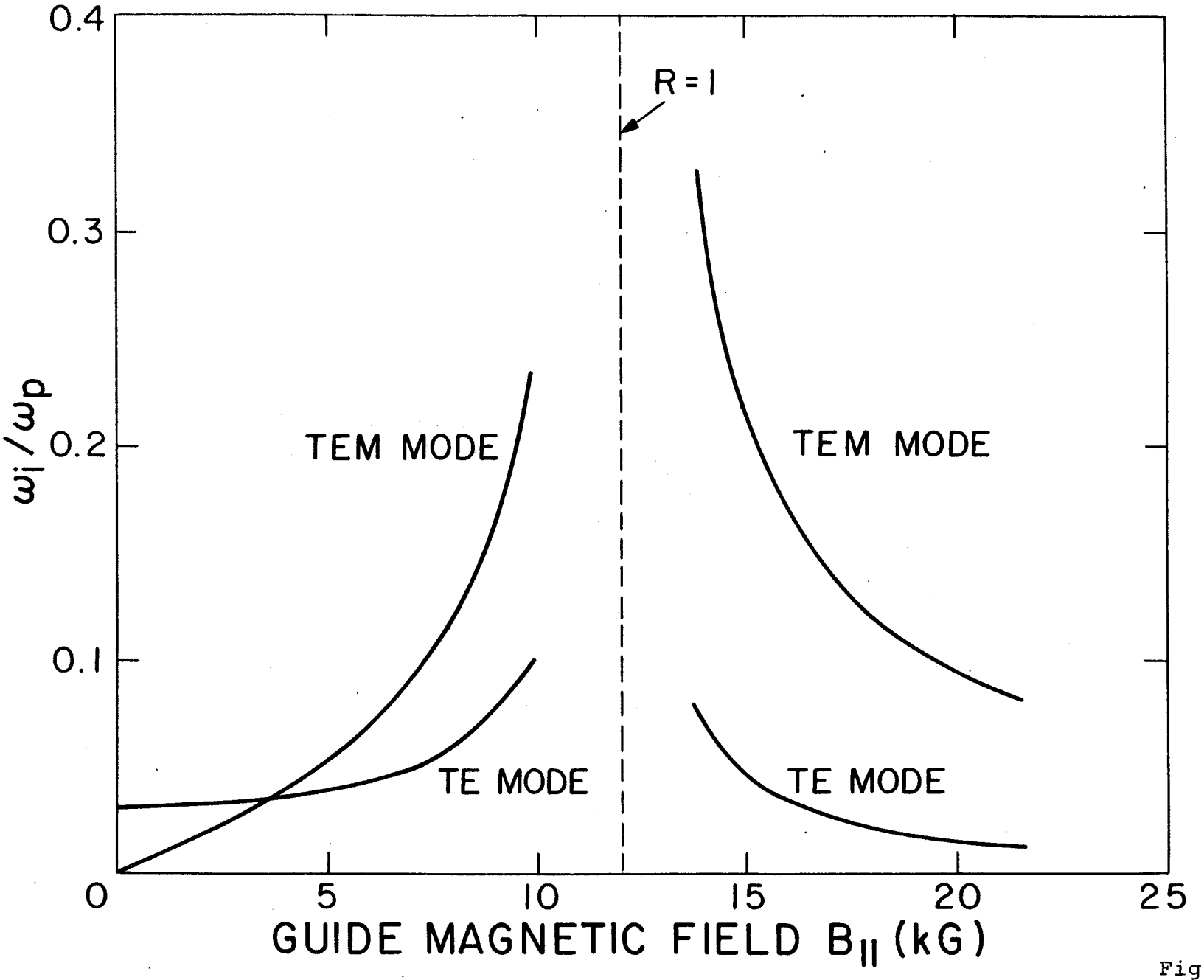

Fig. 6
Yin, Bekefi

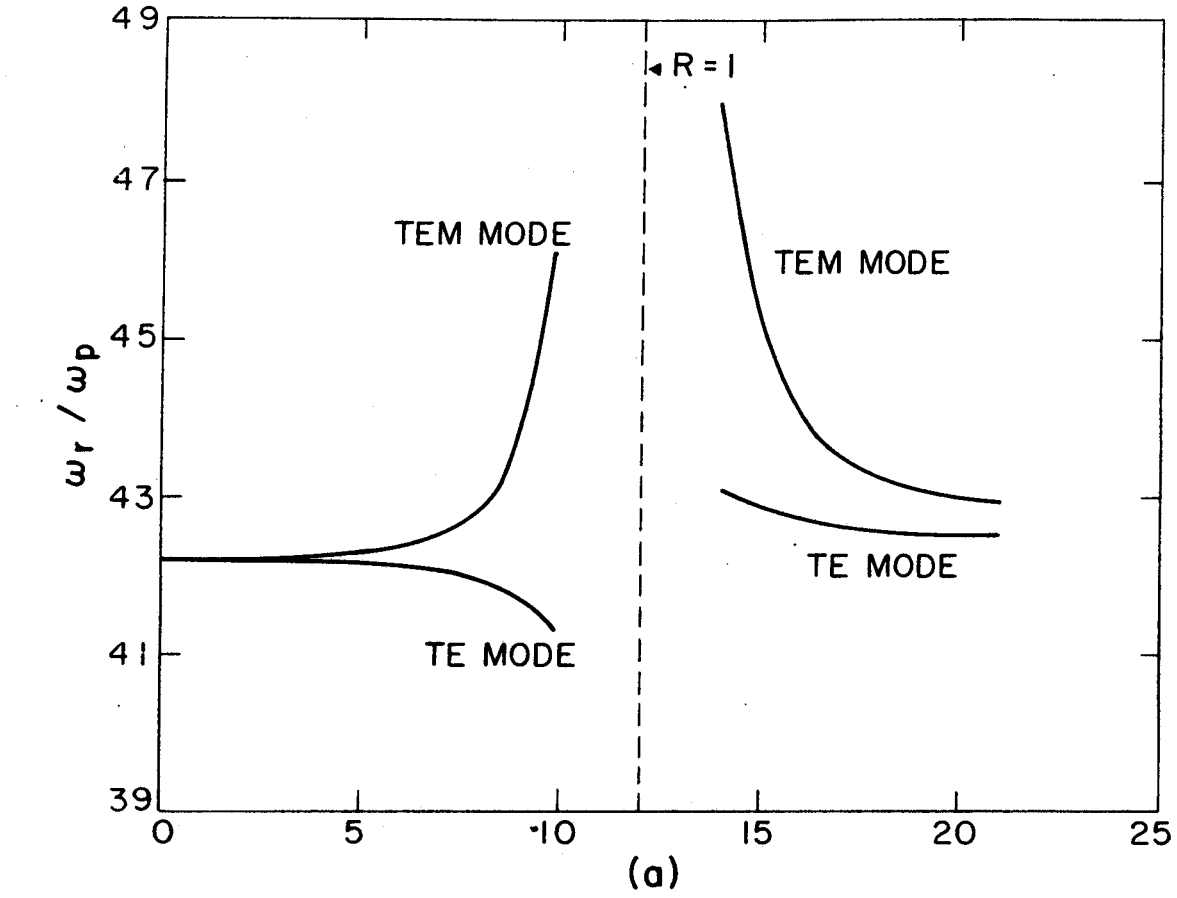

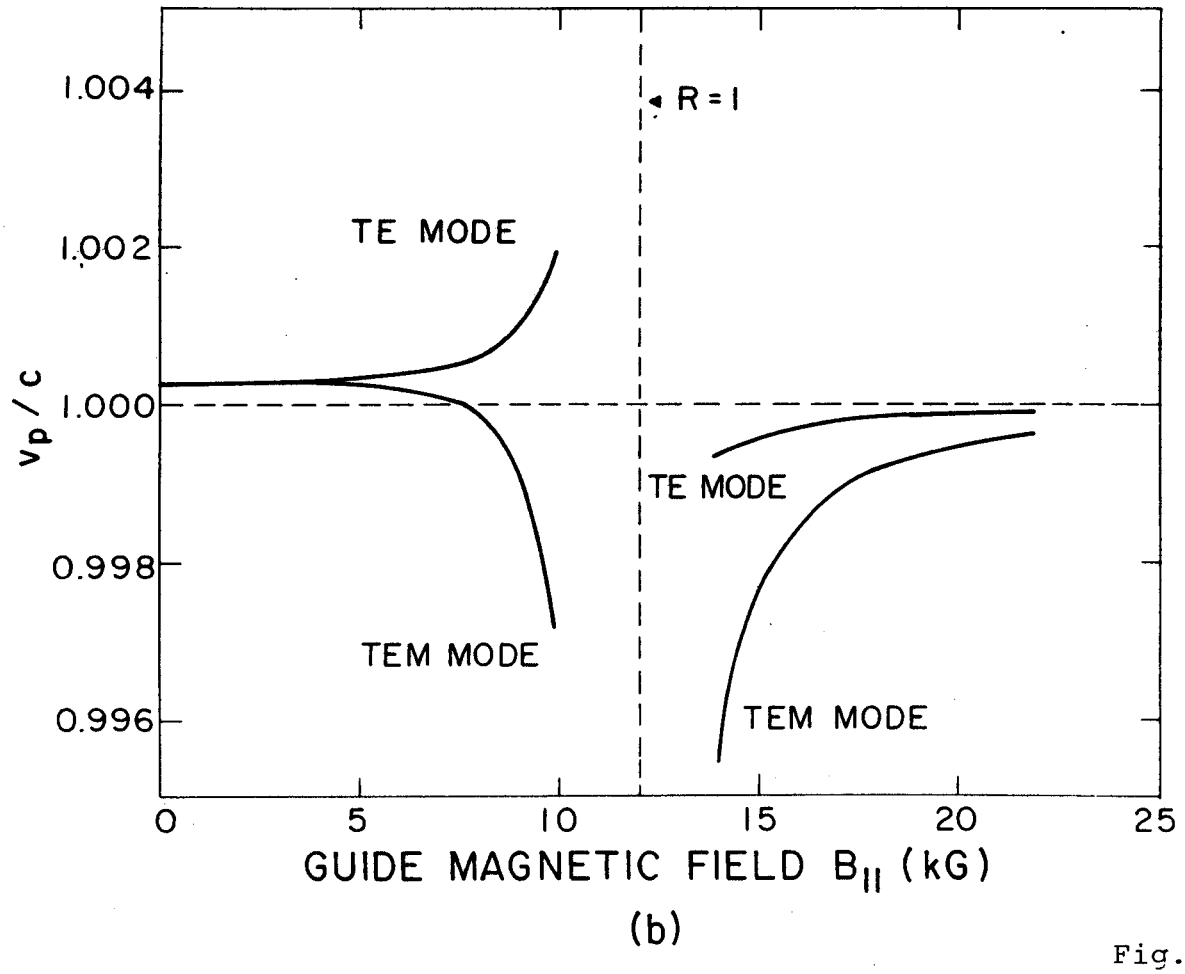

Fig. 7
Yin, Bekefi

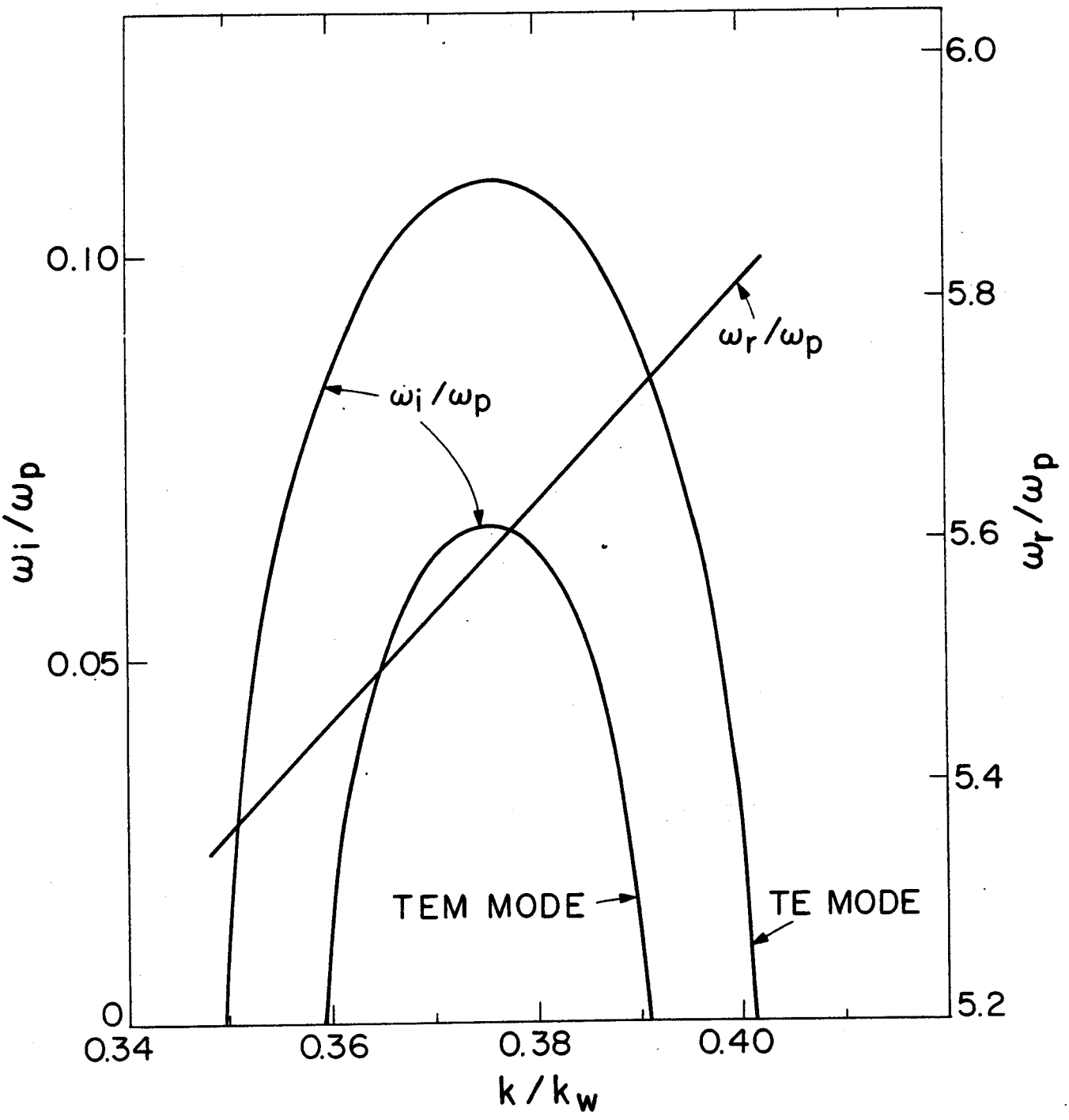

Fig. 8
Yin, Bekefi

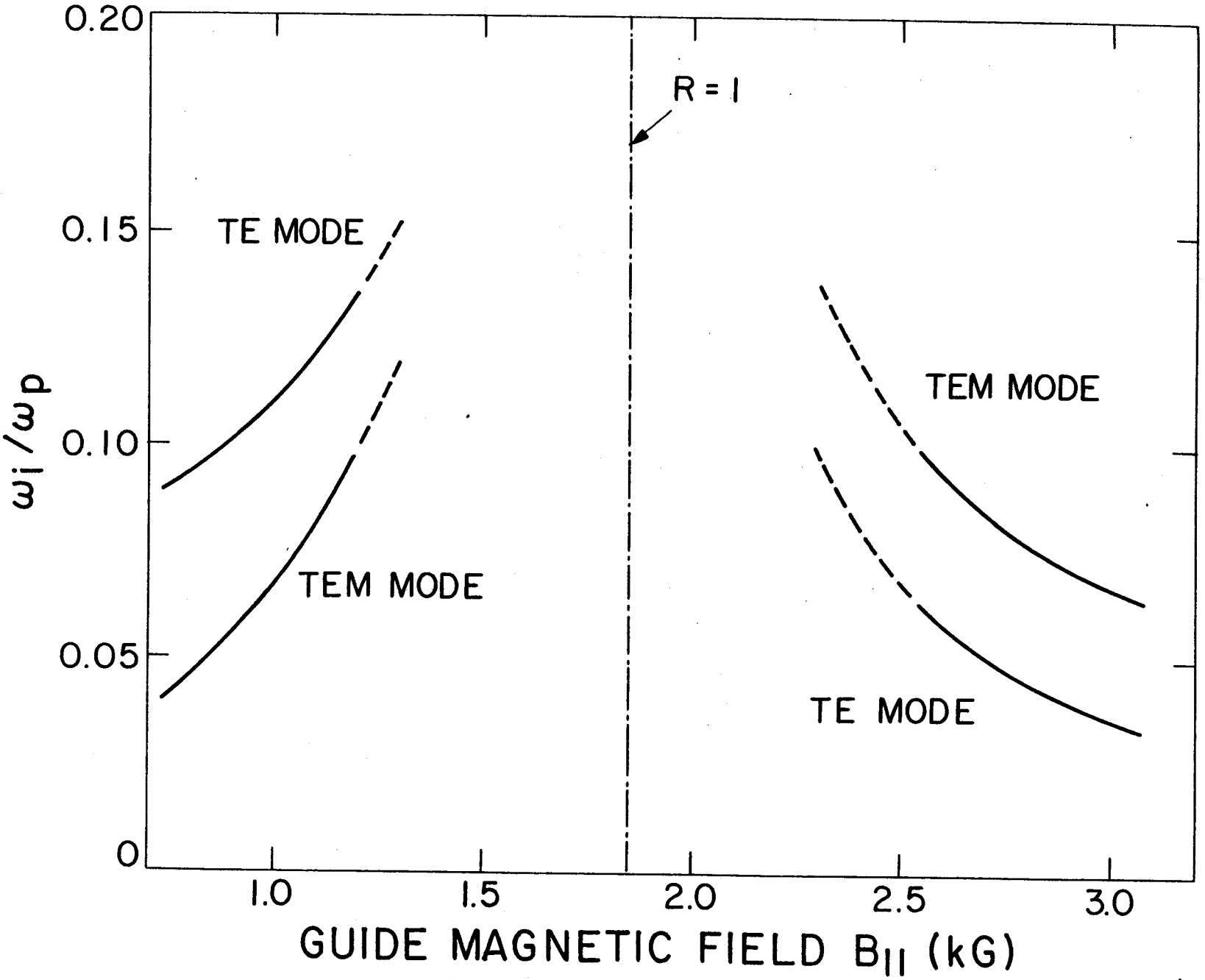

Fin. 9
Yin, Bekefi

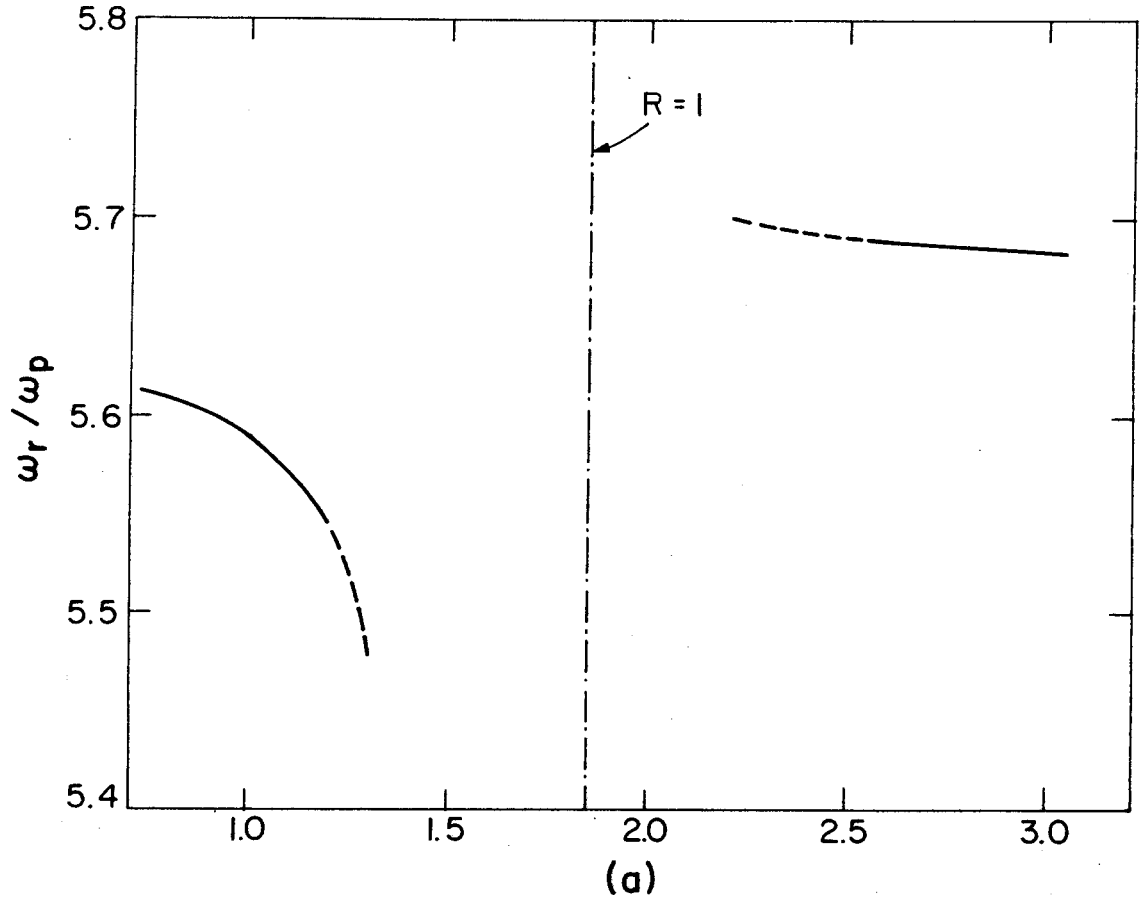

(a)

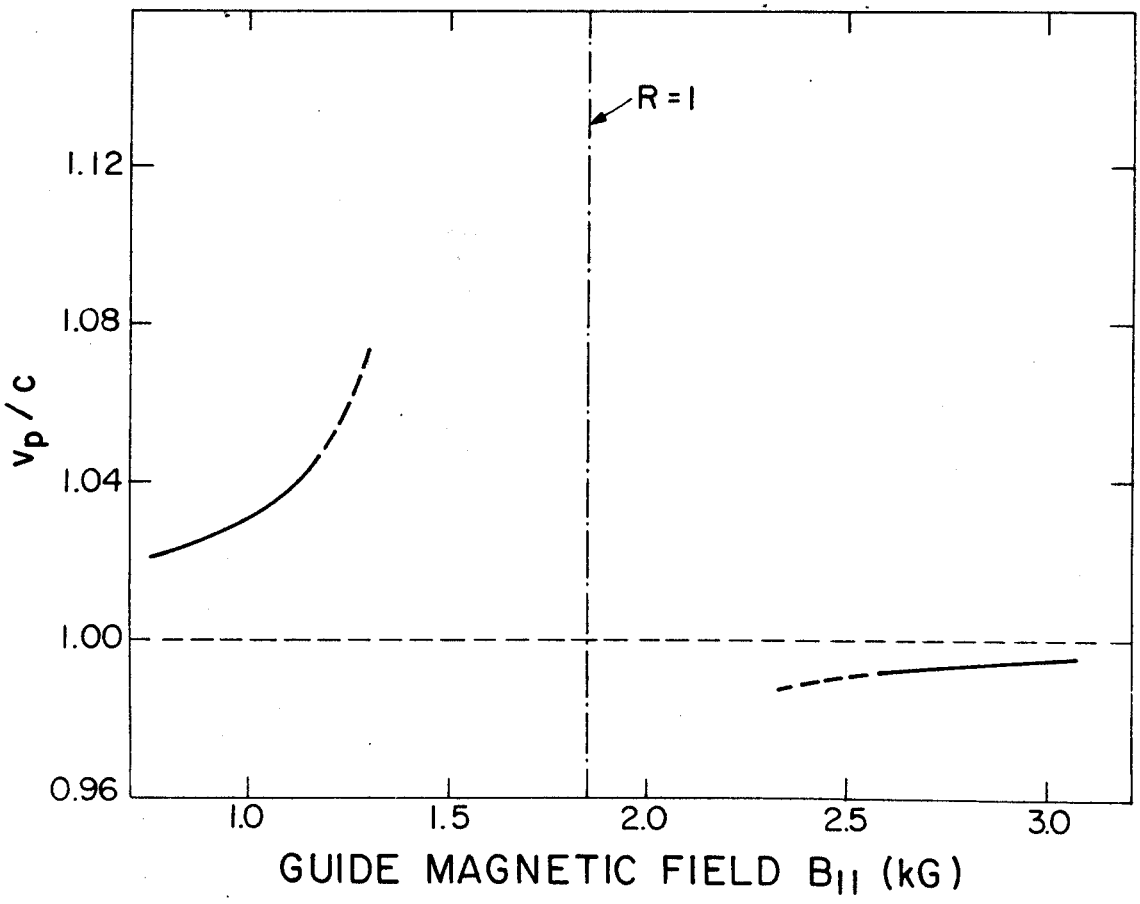

Fig. 10
Yin, Bekefi

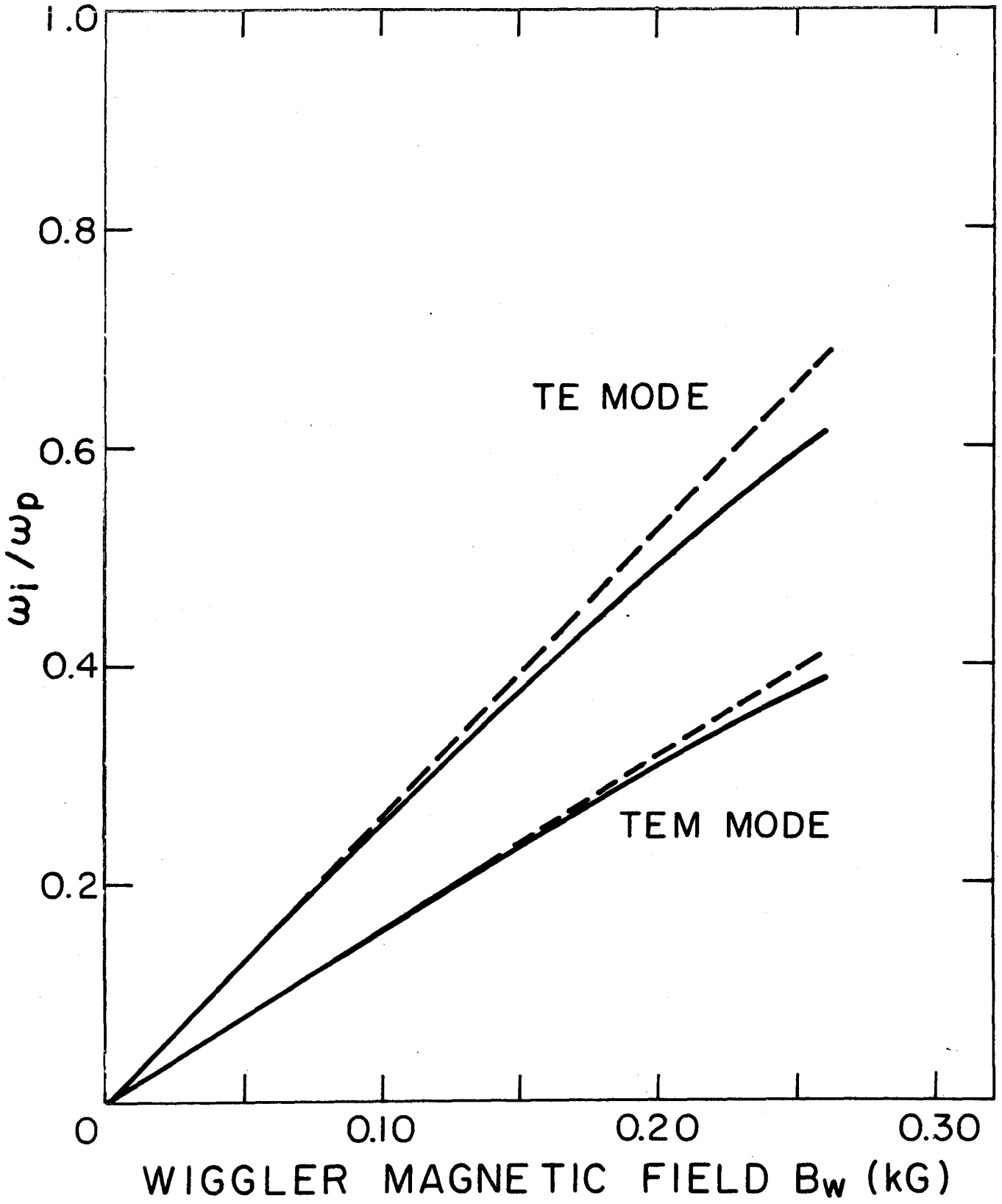

Fig. 11
Yin, Bekefi